Improvement in the Performance of P-Type Tunnel Oxide Passivated Contact Solar Cell With Selective Tunneling Junctions Underneath the Contacts on Front Side

Sourav Sadhukhan, Shiladitya Acharya, Tamalika Panda, Nabin Chandra Mandal, Sukanta Bose, Gourab Das, Santanu Maity, *Senior Member, IEEE*, Partha Chaudhuri, Susanta Chakraborty, *Member, IEEE*, P. Chakrabarti, *Senior Member, IEEE*, and Hiranmay Saha

***Abstract*—Industrial silicon solar cells are now moving further from passivated emitter and rear contact (PERC) toward Tunnel Oxide Passivated contact (TOPCon) technology. The efficiency of the PERC solar cell is improved by TOPCon technology, in which the rear side is fully passivated by an oxide/poly-Si tunneling junction. The performance of a TOPCon solar cell may further be improved by the incorporation of selective tunneling junctions underneath the front contacts. Some fabrications have been reported on a similar structure for an n-type Si substrate but they have not achieved the expected results. Also, a detailed study has not been done yet. Using 3-D sentaurus technology computer aided design (TCAD) simulation software, a detailed analysis has been done on the modified structure through the optimization of the tunnel oxides, the interfaces, the n^{++} poly-Si layer, the selective (SiO_2/n^{++}-poly-Si) tunneling junctions underneath the front contacts, etc., which has not been done earlier. It is seen that a thick n^{++} poly-Si layer causes parasitic absorption of light, whereas a very thin poly-Si layer cannot provide sufficient field for tunneling of carriers. A thicker tunnel oxide produces a high series resistance, whereas a very thin tunnel oxide cannot restrict the minority carriers to reach to the contacts. Therefore, an optimization is required and the optimization is done based on a fabricated bifacial p-TOPCon solar cell reported in the literature with an efficiency of 21.2% and bulk lifetime of 200 μs. After performing all the modifications in the fabricated reference cell and optimizing different parameters, the efficiency is improved by 3.5% in absolute. The efficiency is further improved to 25.4% with the bulk lifetime of 1 ms.**

***Index Terms*—Passivating contacts, pinholes, poly-Si, selective tunneling contacts, tunnel oxide, tunnel oxide passivated contact (TOPCon) solar cell.**

Manuscript received 28 July 2022; revised 4 October 2022 and 1 December 2022; accepted 9 January 2023. Date of publication 3 February 2023; date of current version 20 February 2023. This work was supported by DST Solar PV Hub Phase II at IIEST Shibpur under Project DST/TMD/SERI/HUB/2(G). *(Corresponding authors: Santanu Maity; Susanta Chakraborty.)*

Sourav Sadhukhan, Shiladitya Acharya, Tamalika Panda, Nabin Chandra Mandal, Sukanta Bose, Gourab Das, Santanu Maity, Partha Chaudhuri, and Hiranmay Saha are with the DST-IIEST Solar PV Hub, School of Advanced Materials, Green Energy and Sensor Systems, Indian Institute of Engineering Science and Technology Shibpur, Howrah 711103, India (e-mail: sourav.sadhukhan.rs2018@cegess.iiests.ac.in; shiladitya.rs2017@cegess.iiests.ac.in; tamalikapanda.rs2018@cegess.iiests.ac.in; nabin.rs2021@cegess.iiests.ac.in; sukanta.rs2021@cegess.iiests.ac.in; gourab.rs2019@cegess.iiests.ac.in; santanumaity_4u@rediffmail.com; partha.iacs@gmail.com; hsaha@cegess.iiests.ac.in).

Susanta Chakraborty is with the Department of Computer Science and Technology, IIEST Shibpur, Howrah 711103, India (e-mail: sc.cs@faculty.iiests.ac.in).

P. Chakrabarti is with the Indian Institute of Technology BHU, Varanasi 221005, India, and also with the Indian Institute of Engineering Science and Technology Shibpur, Howrah 711103, India (e-mail: pchakrabarti.ece@iitbhu.ac.in).

Color versions of one or more figures in this article are available at https://doi.org/10.1109/JPHOTOV.2023.3238270.

Digital Object Identifier 10.1109/JPHOTOV.2023.3238270

I. Introduction

An emerging technology called Tunnel Oxide Passivated contact (TOPCon) solar cell with higher conversion efficiency has been most attracted by the industry due to its great potential to replace the existing passivated emitter and rear contact (PERC) technology [1], [2], [3], [4], [5]. The Fraunhofer ISE achieved an efficiency of 25.8% in the laboratory and 23.6% in commercial grade TOPCon solar cells [6], [7]. Conversion efficiencies of 26.1% in small-size wafer in lab scale, 25.2% in industry R&D laboratory, and 24.5% in production line with large cells are also reported [8], [9], [10], [11]. For passivating contact solar cells, the main focus is on n-type TOPCon solar cell due to its higher conversion efficiency than a p-type TOPCon solar cell [1], [8]. But an efficiency of 25.2% in R&D of a p-type TOPCon solar cell is announced by LONGI [12]. The improvement in efficiency of a partial rear contact solar cell is mainly due to the reduction of the recombination of minority carriers at metal–semiconductor interface ($J_{0,\mathrm{met}}$) [13], [14]. In a TOPCon solar cell, $J_{0,\mathrm{met}}$ is substantially suppressed due to full-area rear-side passivation [14], [15], [16], [17], [18]. The performance of TOPCon solar cell may further be improved by incorporating poly-Si-based carrier selective tunneling junctions underneath the front contacts (see Fig. 1).

Fabrication of this type of structure requires few add-ons in the existing process line for TOPCon solar cells. The processes for the deposition of tunnel oxide and poly-Si layers on front side are the same as the layers are deposited on rear side of a TOPCon solar cell. For a p-type substrate, front-side polysilicon is n^{++} and rear-side polysilicon is p^{++}. Now, selective regions, i.e., where the front contacts will be formed, are protected using

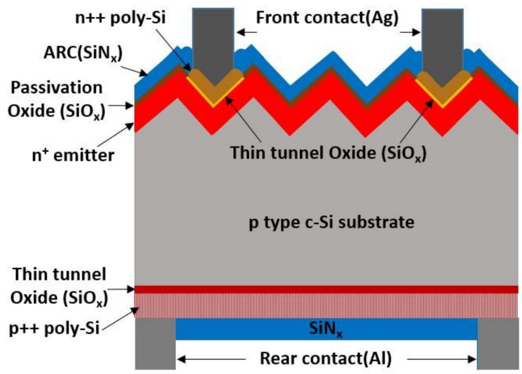

Fig. 1. Bifacial p-type TOPCon solar cell with selective passivating contacts on front side.

UV laser masking or ink-jet masking and the nonmasked regions are etched up to emitter. After that passivating layer stacks are deposited. Implementing this structure on a large area substrate, an efficiency of 23.2% is achieved so far [19], [20]. Similar modification may also be done on the front side of a PERC solar cell [21].

In this work, a fabricated reference bifacial p-TOPCon solar cell is simulated using 3-D Sentaurus technology computer aided design (TCAD) simulation software. Then the performance of the reference TOPCon solar cell is improved step by step through the modifications in the cell structure and optimizations of different parameters. The tunnel oxide thickness, n^{++} poly-Si thickness ($d_{n+\text{ Poly-Si}}$) and doping concentration ($N_{D\text{-poly}}$), ratio of tunneling junction width to front contact width(R), the interfaces and few basic parameters have been optimized through this simulation study.

II. Simulation Models and Parameters

Sentaurus TCAD basically uses empirical equations that make simulation results more practical. It can simulate both optical and electrical simulations simultaneously and can also handle complex device structures with layer thicknesses of few nm to cm [22].

For optical simulation, advanced ray-tracing model [23] is used as an optical solver and quantum yield model [23] is used for optical generations. For all materials (e.g., Si, Si_3N_4, etc.) used in this simulation, complex refractive indices have been considered [23], [24], [25]. In electrical simulation tunneling, current through barrier (oxide) is modeled by Tsu–Esaki model [26]. All other parameters for optical and electrical simulation are briefed in Table I.

III. Results and Discussions

A. Validation of Simulation Model

To validate our model, first we have simulated a bifacial p-type TOPCon solar cell, which has been fabricated by Sebastian Mack et.al. [29]. The dimensions and parameters have been considered for their best cell and the results are compared (see Table II). The parameters for bulk and interface properties of

TABLE I
Physical Parameters for the Simulation Study

Physical Parameters	Value
Front contact	10 µm×40 µm Ag fingers with spacing 1.4mm, shading 2.8%, resistivity 1.51 µΩ·cm, SRV 10^7 cm/s [29].
Front surface	Textured (upright random Pyramids with max. base width 6 µm and height 4 µm) with 80 nm thick ARC(Si_3N_4) [29], [30].
Front emitter	0.3 µm Phosphorus doped with sheet resistance of 90 Ω/sq. [29], [30].
Substrate	p-type Boron dopped mono c-Si wafer with thickness 190 µm; Resistivity of 1.5 Ω·cm [29].
Tunnel oxide layer	SiO_2: $E_g = 8.92$eV, $m_h = 0.33m_0$ and $m_e = 0.42m_0$. [31], [32]. Al_2O_3: $E_g = 7.6$eV, $m_h = 0.36m_0$ and $m_e = 0.40m_0$ [33], [34].
In-diffusion	Boron diffusion from p^{++} poly-Si to the substrate and phosphorus diffusion from n^{++} poly-Si to the substrate considered by analytical doping profile [27], [29].
Rear contact	10 µm×50 µm Al fingers with spacing 0.6 mm, shading 7%, resistivity 2.45 µΩ·cm, SRV = 10^7 cm/s. Rest area is passivated with 80 nm thick Si_3N_4 [29].
SiO_2/Si interface	Acceptor type defects with exponential distribution from 0.4 to 0.5 eV below the CB with peak concentration 1E10 cm^{-2}, Fixed charge = +1E11 cm^{-2} [35], [36].
Poly-Silicon layer	Both Donor and Acceptor type defects at 0.37 eV above VB and below CB, respectively [37], [38]. p+ poly-Si thickness = 240 nm[29].
SiO_2/poly-Si interface	Acceptor (p-poly) and Donor (n-poly) type defects at 0.45 eV below CB with concentration 1E12 cm^{-2}, Fixed charge = +2E11 cm^{-2}[39], [40].
Mobility	Klaassen mobility model [41], [42].
Other models	Lifetime, recombination, BGN, etc., models are considered as per literature of Altermatt. [43]
Light source	AM1.5G with intensity 1 kW/m^2 (ASTM G173-03) [44].
Device Temperature	300 K

TABLE II
Comparison of Results for Fabricated [18] and Simulated (With the Parameters in Table I) P-TOPCon Solar Cells

Cell Type	Voc (mV)	Jsc (mA/cm^2)	FF (%)	η (%)	R_s (Ω·cm^2)
Fabricated Ref.	671.0	39.5	80.0	21.2	0.55
Simulated Ref.	674.8	39.3	80.1	21.2	0.53

different layers are taken from different literature works, which are briefed in Table I. The tunnel oxide thickness (d_{SiO2}) of 1.2 nm, pinholes of radius 4 nm, and density 1E4 cm^{-2} in the tunnel oxide layer(SiO_2), p^{++} poly-Si doping of 8E19 cm^{-3}, and bulk lifetime (τ_{Bulk}) of 200 μs is considered to achieve the outputs of fabricated reference cell.

The open-circuit voltage (*V*oc), short-circuit current (*I*sc), series resistance (R_s), fill factor (FF), etc., of a TOPCon solar cell are very much dependent on pinhole radius, pinhole nature, pinhole density, rear tunnel oxide (SiO_2) thickness, and poly-Si layer [27]. So, these parameters should be optimized, and for a p-TOPCon solar cell, these parameters are optimized in the previous work [28], which is not reported here. The optimized parameters are: pinhole radius = 4 nm, pinhole density = 5E6 cm^{-2}, tunnel oxide thickness (d_{SiO2}) = 1.2 nm, p^{++} poly-Si thickness = 240 nm, and doping = 8E19 cm^{-3}. Pinholes are 60% completely through and 40% partially through. Considering these optimized values, the efficiency of the simulated reference cell has improved to 22.6% with *V*oc of 673.7 mV, *J*sc of 39.6 cm·A/cm^2, FF of 84.6%, and series resistance (R_s) of 0.16 $\Omega \cdot cm^2$ (see Table IV). The improvement in the efficiency of simulated reference TOPCon solar cell is mainly due to higher FF, which results from lower series resistance (R_s) of the cell.

B. Improvement in Front-Side Passivation and Bulk Doping

For the fabricated p-TOPCon solar cell, the front side is textured and passivated with nitride and Si_3N_4/Si interface possess higher defects [45] than SiO_2/Si interface. After PSG removal, the wafers are annealed [29], so a thin SiO_2 layer (1–2 nm) may be formed or deposited (∼5 nm) [30] before deposition of silicon nitride on front side. The low value of open-circuit voltage (*V*oc) of 671.0 mV may be due to higher defects at the SiO_2/Si interface. Therefore, in the simulation, the front SiO_2/Si interface is considered of poor quality with high interface defects of 2E11 cm^{-2} and obtained *V*oc of 673.7 mV (see Table II). Now front SiO_2/Si interface can be improved by considering acceptor-type defects with exponential distribution from 0.4 to 0.5 eV below the CB with peak concentration 1E10 cm^{-2}, electron capture cross-section = 1E-14 cm^2, hole capture cross-section = 1E-14 cm^2, and fixed charge = +1E11 cm^{-2}, which is most common and reported in literatures (see Table I). This reduces the Shockley–Read–Hall (SRH) [46] recombination at SiO_2/Si interface which in turn reduces recombination current density (J_0) by 94.5 fA/cm^2 and improves *V*oc to 690.1 mV, efficiency to 23.2% with R_s = 0.17 $\Omega \cdot cm^2$.

The performance is further improved by optimizing the Boron (B) doping in the substrate ($N_{A,subs}$). The B doping concentration is varied from 8E15 cm^{-3} to 6E16 cm^{-3}. Highest efficiency of 23.8% is achieved at $N_{A,subs}$ 4E16 cm^{-3}. With the increase of B doping concentration in the substrate from 1E16 cm^{-3} mainly, the short-circuit-current density (*J*sc) increases and reaches to 40.7 mA/cm^2 at $N_{A,subs}$ of 4E16 cm^{-3}. Further increase of $N_{A,subs}$ results in decrease of *J*sc. On the other hand, with the decrease of $N_{A,subs}$ from 1E16 cm^{-3}, *J*sc decreases. The increase in *J*sc is mainly due to the improvement in tunnel current [26] and the conductivity of the substrate. For optimized $N_{A,subs}$ (4E16 cm^{-3}), R_s is reduced to 0.15 $\Omega \cdot cm^2$ and FF is improved to 84.9%.

C. Improvement With Al_2O_3 Tunnel Oxide on Rear Side

SiO_2 has been used as the tunneling oxide but it has positive fixed charge ∼ +1E11 cm^{-2} (see Table I), which induces minority electrons on the rear side and increases SRH recombination at SiO_2/p-Si interface. This recombination loss can be reduced by considering a tunneling oxide which has negative fixed charges. In this context, Al_2O_3 has been used as tunnel oxide [47], [48] with tunneling masses $m_h = 0.36 m_0$, $m_e = 0.40\, m_0$ and negative fixed charge ∼ −5E12 cm^{-2} (see Table I). Now, Al_2O_3 layer is

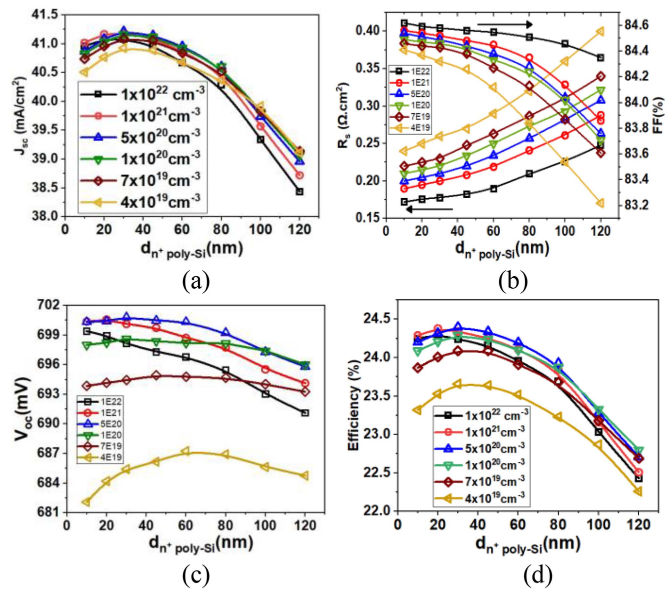

Fig. 2. Variation of (a) *J*sc (in mA/cm^2), (b) R_s (in mA/cm^2) and FF (in %), (c) *V*oc (mV), and (d) efficiency (in %) with $d_{n+\ poly\text{-}Si}$ (in nanometer) taking $N_{D\text{-}poly}$ (in cm^{-3}) as parameter.

optimized to achieve better performance of the cell. The highest efficiency of 23.9% is achieved with *V*oc of 693.3 mV, *J*sc of 40.8 mA/cm^2, FF of 84.5%, and R_s of 0.2 $\Omega \cdot cm^2$ for oxide thickness of 1.2 nm, pinhole radius of 4 nm, pinhole density of 5E6 cm^{-2}(60% completely through and 40% partially through), p^{++} poly-Si doping concentration of 8E19 cm^{-3}, p^{++} poly-Si thickness of 240 nm, p substrate doping of 4E16 cm^{-3}, n^+ emitter doping of 2E19 cm^{-3} and bulk lifetime of 200 μs.

D. Further Improvement by N-TOPCon Structure Underneath the Front Contact

Now for further improvement in conventional p-TOPCon solar cell, selective n-TOPCon structures are formed in between front contacts and emitter (see Fig. 1). Initially, $d_{ox\text{-}F}$ = 1.2 nm, $d_{n+\ poly\text{-}Si}$ = 30 nm, $N_{D\text{-}poly}$ = 1E20 cm^{-3}, the ratio of tunneling junction width to front contact width (R) = 2 and in the tunnel oxide layer on front-side pinholes with radius 4 nm, and density of 1E7 cm^{-2} are considered [19], [20], [28]. In the next steps, the above-mentioned parameters for n-TOPCon structure are optimized. Considering these initial parameters, the efficiency is improved to 24.3% with *V*oc of 698.6 mV, *J*sc of 41.2 mA/cm^2, FF of 84.5% and R_s of 0.22 $\Omega \cdot cm^2$.

1) Thickness and Doping Optimization of Front n^{++} Poly-Si Layer: The thickness of front n^{++} poly-Si is varied from 10 to 120 nm, considering phosphorus doping concentration ($N_{D\text{-}poly}$) as parameter which is varied from 4E19 cm^{-3} to 1E22 cm^{-3} (see Fig. 2). In this step, front tunnel oxide thickness is kept constant at 1.2 nm.

It has been seen that with increase in n^{++} poly-Si thickness, initially *J*sc increases and after a certain thickness it starts to decrease [see Fig. 2(a)]. This is because thin polysilicon layer cannot provide sufficient field for majority electrons to tunnel through oxide barrier. It is also seen that the minimum thickness for sufficient field for tunneling depends on the doping concentration ($N_{D\text{-poly}}$). In Fig. 2(a), it is seen that the peak of *J*sc shifts toward thinner polysilicon ($d_{n+\text{ Poly-Si}}$) with higher $N_{D\text{-poly}}$. The highest *J*sc achieved is 41.2 mA/cm^2 for $d_{n+\text{ poly-Si}}$ 30–45 nm and $N_{D\text{-poly}}$ 1E20–1E21 cm^{-3} range. For $N_{D\text{-poly}} >$ 1E21 cm^{-3}, highest *J*sc cannot be reached even for thinner poly-Si due to unavoidable Auger recombination and free carrier absorption [49]. Again the decrease in *J*sc with thicker poly-Si, which is different for different $N_{D\text{-poly}}$, is due to absorption of incident light in the poly-Si layer. Higher the thickness, higher is the absorption, and as poly-Si layer is defective (see Table I), a large number of generated minority holes are recombined without contributing to the total current. It is seen that light can enter into n^{++} poly-Si region due to inclined incidence of light [50] and diffraction of light [51] at metal/silicon-nitride interface even if it is covered by the metal fingers.

In Fig. 2(b), it is seen that R_s increases with increase in $d_{n+\text{ poly-Si}}$ in a nonlinear manner and the slope is steeper for thicker poly-Si. R_s increases with n^{++}poly-Si thickness because carriers have to travel longer path before collection. Also, the slope of R_s for thicker poly-Si is steeper because the electric field becomes weaker with increasing thickness of poly-Si leading to higher recombination of minority holes. Again, the slope is steeper with lower $N_{D\text{-poly}}$. It is well known that higher is the R_s, lower is the FF of the cell. We can see in Fig. 2(b) that with increase in $d_{n+\text{ poly-Si}}$, the FF of the cell decreases. Similar to R_s, the slope of decrement is steeper with lower $N_{D\text{-poly}}$. In the range of variation, we achieved lowest R_s of 0.17 Ω·cm^2, highest FF of 84.6% at $d_{n+\text{ poly-Si}} = 10$ nm and $N_{D\text{-poly}} =$ 1E22 cm^{-3} and highest R_s of 0.41 Ω·cm^2, lowest FF of 83.1% at $d_{n+\text{ poly-Si}} = 120$ nm, and $N_{D\text{-poly}} =$ 4E19 cm^{-3}.

*V*oc of the cell also decreases with increase in $d_{n+\text{ poly-Si}}$ but the slope of decrement is flat [see Fig. 2(c)]. The decrease of *V*oc with thicker poly-Si is due to higher SRH recombination in the poly-Si region. Also, very high doping in poly-Si layer results in lower *V*oc due unavoidable auger recombination. Due to different nature of variations of *J*sc, *V*oc, FF, and R_s, the efficiency of the cell varies, as shown in Fig. 2(d). The efficiency increases with increase in $d_{n+\text{ poly-Si}}$ and reaches to a peak then decreases. The peak efficiency again increases with increase in $N_{D\text{-poly}}$ and reaches to maximum then decreases. The highest efficiency achieved in this stage is 24.4% at $d_{n+\text{ poly-Si}} = 20$ nm, $N_{D\text{-poly}} =$ 1E21 cm^{-3} and at $d_{n+\text{ poly-Si}} = 30$ nm, $N_{D\text{-poly}} =$ 5E20 cm^{-3}.

2) Optimization of Front Oxide Thickness and Ratio of Tunneling Junction Width to Front Contact Width: To achieve the best performance, front tunnel oxide thickness (dox_F) and the ratio of tunneling junction width to front contact width (R) should be optimized. For this purpose, dox_F is varied from 1.0 to 1.7 nm considering R as parameter which is varied from 1 to 3.

As dox_F increases from 1 nm, initially *J*sc increases and reaches to a maximum and then decreases [see Fig. 3(a)]. Initially, when front tunnel oxide is very thin, it allows minority holes to transport from emitter to n^{++} poly-Si and Ag contacts which are lost due to recombination without contributing to output current. As front tunnel oxide gets thicker, it blocks minority hole to transport from emitter to front contact and these holes reach to the junction and gets separated contributing to the output current. Hence, *J*sc increases with thicker front tunnel oxide. But it happens up to a certain thickness; after that tunneling, probability [26] of majority electrons decreases which in turn decreases output current. Again as R increases from 1 that is when tunneling junction (oxide + n^{++} poly-Si), width becomes greater than the front contact width then *J*sc decreases rapidly. This is due to the absorption of light in the n^{++} poly-Si region. The highest *J*sc achieved is 41.3 mA/cm^2 for R = 1 and dox_F = 1.2–1.5 nm. In Fig. 3(a), it is also seen that R_s increases with increase in dox_F. This is because of the reduction of tunnel current with increment of dox_F [26]. This increase in R_s results in a lower value of FF of the cell. The nature of variation of *V*oc with dox_F and R is similar to *J*sc. Therefore, depending on the variations of *J*sc, *V*oc, and FF, the efficiency of the cell varies, as shown in Fig. 3(b). The highest efficiency achieved in this step is 24.6% with *V*oc = 704.5 mV, *J*sc = 41.3 mA/cm^2, FF = 84.5%, and R_s = 0.21 Ω·cm^2 for R = 1, dox_F = 1.5 nm $d_{n+\text{ poly-Si}} = 30$ nm, $N_{D\text{-poly}} =$ 5E20 cm^{-3}, and $\tau_{\text{Bulk}} = 200$ μs.

The efficiency is further improved by decreasing the front contact percentage from 2.8% to 2%. Further decrement of front contact percentage decreases the efficiency. The increment in efficiency is due to the reduction of front shading by metal contacts. But very low percentage of front contact increases the contact resistance and carrier crowding in the contacts and, hence, efficiency decreases. The highest efficiency achieved is 24.7% with *V*oc = 705.0 mV, *J*sc = 41.5 mA/cm^2, FF = 84.5%, and R_s = 0.22 Ω·cm^2 for the optimized parameters listed in Table III. Therefore, performing all the improvements in the reference TOPCon solar cell, the efficiency is improved by 3.5%.

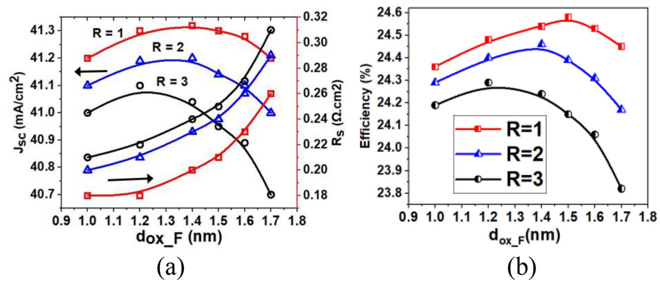

Fig. 3. Variation of (a) *J*sc (in mA/cm^2) and R_s (in Ω·cm^2) and (b) efficiency (in %) with front tunnel oxide thickness (dox_F in nanometer) taking ratio of tunneling junction width to front contact width (R) as parameter.

TABLE III
OPTIMIZED PARAMETERS

Parameters	Value
Resistivity of Substrate (p-type)	0.9 Ω·cm (4×10^{16} cm^{-3})
sheet resistance of front emitter	90 Ω/sq.
Front contact	10 μm×35 μm with spacing 1.7 mm, and shading 2%.
$d_{n+\text{ poly-Si}}$	30 nm
$N_{D\text{-poly}}$ / $N_{A\text{-poly}}$	5×10^{20} cm^{-3} / 8×10^{19} cm^{-3}
d_{ox_F} / d_{ox_R}	1.5 nm / 1.2 nm
Rear contact	10 μm×50 μm with spacing 0.6 mm, and shading 7%.

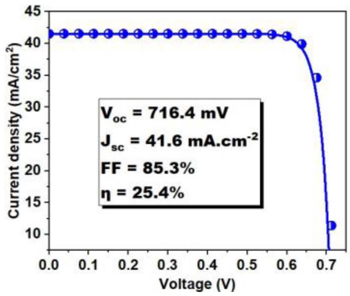

Fig. 4. Current density (*J*)–Voltage (*V*) characteristics of the best cell for front contact percentage = 2%, R = 1, $dox_{\_F}$ = 1.5 nm $d_{n+ \text{ poly-Si}}$ = 30 nm, $N_{\text{D-poly}}$ = 5E20 cm^{-3}, and τ_{Bulk} = 1 ms.

TABLE IV
SUCCESSIVE IMPROVEMENTS

Steps	Efficiency
Initial reference cell (both fabricated and simulated)	21.2%
After optimization of tunnel oxide thickness (SiO_2), pinhole radius, density, and nature	22.6
After front-side passivation improvement	23.2
After optimizing substrate doping	23.8
Using Al_2O_3 as tunnel layer on the rear side	23.9
Integration of front poly without optimization	24.3
After front poly thickness and doping optimization	24.4
After optimizing oxide thickness	24.6
After decreasing metal area coverage on front side	24.7
After increasing bulk lifetime from 200 µs to 1 ms	25.4

This efficiency can further be improved to 25.4% with *V*oc of 716.4%, *J*sc of 41.6 mA/cm^2, FF of 85.3%, R_s of 0.34 Ω·cm^2, and overall reverse saturation current density (J_0) of 40.5 fA/cm^2 by increasing the bulk lifetime(τ_{Bulk}) to 1 ms (see Fig. 4).

IV. CONCLUSION

To achieve optimum performance of a TOPCon solar cell oxide/Si interface, tunnel oxide thickness, density, nature, and radius of pinholes in the oxide layer and the poly-Si layer should be optimized. The SiO_2 tunnel layer in a p-TOPCon solar cell may be replaced with a tunnel oxide layer that has negative fixed charge, provided that the hole tunneling mass is not sufficiently large and the oxide/p-c-Si interface does not have significant interface defects (e.g., Al_2O_3). The performance of a p-TOPCon solar cell can further be improved by passivating the front contacts with n-type tunneling junctions. As the n^{++} poly-Si/SiO_2 layer stack is on the front side and light enters in the cell through front side, hence the optimization of tunnel oxide thickness, n^{++} poly-Si thickness and doping and the width of SiO_2/n^{++}poly-Si tunneling junctions underneath the front contacts become important. Optimizing all the parameters, the efficiency of the reference p-TOPCon solar cell has been improved from 21.2% to 25.4%, and the reverse saturation current density is reduced to 40.4 fA/cm^2 from 221.4 fA/cm^2. The successive improvements are indicated in Table IV.

This efficiency may further be improved by increasing the bulk lifetime. In fabrication of this structure, the main challenges are the control of the width of the openings and deposition of thin poly-Si with high doping concentration of phosphorus (such as 5E20 cm^{-3} for 30 nm poly-Si, 1E21 cm^{-3} for 20 nm poly-Si, etc.) on the front side which is textured. Overall, there is a scope of improvisation of TOPCon solar cell by this type of structure but it requires lots of experiments.

REFERENCES

[1] S. W. Glunz et al., “Silicon-based passivating contacts: The TOPCon route,” *Prog. Photovolt., Res. Appl.,* pp. 1–19, Dec. 2021, doi: 10.1002/pip.3522.
[2] D. Yan et al., “Silicon solar cells with passivating contacts: Classification and performance,” *Prog. Photovolt., Res. Appl.,* May 2022, doi: 10.1002/pip.3574.
[3] A. Richter et al., “Design rules for high-efficiency both-sides-contacted silicon solar cells with balanced charge carrier transport and recombination losses,” *Nature Energy*, vol. 6, no. 4, pp. 429–438, 2021.
[4] R. Peibst et al., “On the chances and challenges of combining electron-collecting nPOLO and hole-collecting Al-p+ contacts in highly efficient p-type c-Si solar cells,” *Prog. Photovolt., Res. Appl.*, Feb. 2022, doi: 10.1002/pip.3545.
[5] B. Steinhauser et al., “Investigation of the defect distribution of laser contact opening applied to poly-Si/SiNx stacks,” *Physica Status Solidi (A)*, vol. 219, no. 8, Apr. 2022, Art. no. 2100832.
[6] B. Grübel et al., “Progress of plated metallization for industrial bifacial TOPCon silicon solar cells,” *Prog. Photovolt., Res. Appl.*, vol. 30, no. 6, pp. 615–621, Jun. 2022.
[7] A. Richter et al., “Design rules for high-efficiency both-sides-contacted silicon solar cells with balanced charge carrier transport and recombination losses,” *Nature Energy*, vol. 6, no. 4, pp. 429–438, 2021.
[8] M. A. Green et al., “Solar cell efficiency tables (Version 58),” *Prog. Photovolt., Res. Appl.*, vol. 29, 2021, Art. no. NREL/JA-5900-80028.
[9] D. Chen et al., “24.58% total area efficiency of screen-printed, large area industrial silicon solar cells with the tunnel oxide passivated contacts (i-TOPCon) design,” *Sol. Energy Mater. Sol. Cells*, vol. 206, Mar. 2020, Art. no. 110258.
[10] Y. Chen et al., “Mass production of industrial tunnel oxide passivated contacts (i-TOPCon) silicon solar cells with average efficiency over 23% and modules over 345 W,” *Prog. Photovolt., Res. Appl.*, vol. 27, no. 10, pp. 827–834, 2019.
[11] F. Haase et al., “Laser contact openings for local poly-Si-metal contacts enabling 26.1%-efficient POLO-IBC solar cells,” *Sol. Energy Mater. Sol. Cells*, vol. 186, pp. 184–193, Nov. 2018.
[12] “LONGi sets another record for p-type TOPCon solar cell efficiency,” Jul. 22, 2021. [Online]. Available: https://www.longi.com/en/news/7056/
[13] A. Cuevas, “Electrons and holes in solar cells with partial rear contacts,” *Prog. Photovolt., Res. Appl.*, vol. 22, no. 7, pp. 764–774, 2014.
[14] F. Feldmann et al., “Tunnel oxide passivated contacts as an alternative to partially rear contacts,” *Sol. Energy Mater. Sol. Cells*, vol. 131, pp. 46–50, 2014.
[15] C. Messmer et al., “Efficiency roadmap for evolutionary upgrades of PERC solar cells by TOPCon: Impact of parasitic absorption,” *IEEE J. Photovolt.*, vol. 10, no. 2, pp. 335–342, Mar. 2020.
[16] U. Römer et al., “Recombination behavior and contact resistance of n+ and p+ poly-crystalline Si/mono-crystalline Si junctions,” *Sol. Energy Mater. Sol. Cells*, vol. 131, pp. 85–91, 2014.
[17] C. Reichel et al., “Polysilicon contact structures for silicon solar cells using atomic layer deposited oxides and nitrides as ultra-thin dielectric interlayers,” *Prog. Photovolt., Res. Appl.*, vol. 30, no. 3, pp. 288–299, 2022.
[18] D. Yan, A. Cuevas, S. P. Phang, Y. Wan, and D. Macdonald, “23% efficient p-type crystalline silicon solar cells with hole-selective passivating contacts based on physical vapor deposition of doped silicon films,” *Appl. Phys. Lett.*, vol. 113, no. 6, 2018, Art. no. 061603.
[19] S. Singh et al., “Large area co-plated bifacial n-PERT cells with polysilicon passivating contacts on both sides,” *Prog. Photovolt., Res. Appl.*, vol. 30, no. 8, pp. 899–909, Aug. 2022.
[20] B. Yu et al., “Selective tunnel oxide passivated contact on the emitter of large-size n-type TOPCon bifacial solar cells,” *J. Alloys Compounds*, vol. 870, 2021, Art. no. 159679.
[21] S. Yuan et al., “Passivated emitter and rear cell silicon solar cells with a front polysilicon passivating contacted selective emitter,” *Physica Status Solidi (RRL)–Rapid Res. Lett.*, vol. 15, no. 7, 2021, Art. no. 2100057.

[22] Y.-C. Wu and Y.-R. Jhan, "Introduction of Synopsys Sentaurus TCAD simulation," in *3D in TCAD Simulation for CMOS Nanoeletronic Devices*. Berlin, Germany: Springer, 2018, pp. 1–17.

[23] "Synopsys Sentaurus TCAD user manual," version S-2021.06, Jun. 2021.

[24] PV Light House, "Refractive index library," 2022. [Online]. Available: https://www.pvlighthouse.com.au/refractive-index-library

[25] "Refractive index info," 2022. [Online]. Available: https://refractiveindex.info/

[26] R. Tsu and L. Esaki, "Tunneling in a finite superlattice," *Appl. Phys. Lett.*, vol. 22, no. 11, pp. 562–564, 1973.

[27] N. Folchert, R. Peibst, and R. Brendel, "Modeling recombination and contact resistance of poly-Si junctions," *Prog. Photovolt. Res. Appl.*, vol. 28, no. 12, pp. 1289–1307, Dec. 2020.

[28] S. Sadhukhan et al., "Detailed study on the role of nature and distribution of pinholes and oxide layer on the performance of tunnel oxide passivated contact (TOPCon) solar cell," *IEEE Trans. Electron Devices*, vol. 69, no. 10, pp. 5618–5623, Oct. 2022.

[29] S. Mack, D. Herrmann, M. Lenes, M. Renes, and A. Wolf, "Progress in p-type tunnel oxide-passivated contact solar cells with screen-printed contacts," *Sol. RRL*, vol. 5, no. 5, 2021, Art. no. 2100152.

[30] N. C. Mandal et al., "Evolution of PERC from Al-BSF: Optimization based on root cause analysis," *Appl. Phys. A*, vol. 126, no. 7, pp. 1–10, Jun. 2020.

[31] M. I. Vexler, S. E. Tyaginov, and A. F. Shulekin, "Determination of the hole effective mass in thin silicon dioxide film by means of an analysis of characteristics of a MOS tunnel emitter transistor," *J. Phys., Condens. Matter*, vol. 17, no. 50, 2005, Art. no. 8057.

[32] A. Schenk and G. Heiser, "Modeling and simulation of tunneling through ultra-thin gate dielectrics," *J. Appl. Phys.*, vol. 81, no. 12, pp. 7900–7908, 1997.

[33] K. Gloos, P. J. Koppinen, and J. P. Pekola, "Properties of native ultrathin aluminium oxide tunnel barriers," *J. Phys., Condens. Matter*, vol. 15, no. 10, 2003, Art. no. 1733.

[34] T. V. Perevalov, A. V. Shaposhnikov, and V. A. Gritsenko, "Electronic structure of bulk and defect α-and γ-Al2O3," *Microelectronic Eng.*, vol. 86, no. 7/9, pp. 1915–1917, 2009.

[35] W. D. Eades and R. M. Swanson, "Calculation of surface generation and recombination velocities at the Si-SiO2 interface," *J. Appl. Phys.*, vol. 58, no. 11, pp. 4267–4276, 1985.

[36] H. Flietner, W. Füssel, N. D. Sinh, and H. Angermann, "Density of states and relaxation spectra of etched, H-terminated and naturally oxidized Si-surfaces and the accompanied defects," *Appl. Surf. Sci.*, vol. 104, pp. 342–348, 1996.

[37] J. Y. W. Seto, "The electrical properties of polycrystalline silicon films," *J. Appl. Phys.*, vol. 46, no. 12, pp. 5247–5254, 1975.

[38] S. D. Brotherton, J. R. Ayres, and N. D. Young, "Characterisation of low temperature poly-Si thin film transistors," *Solid-State Electron.*, vol. 34, no. 7, pp. 671–679, 1991.

[39] C.-Y. Wu and C.-F. Chen, "Transport properties of thermal oxide films grown on polycrystalline silicon—modeling and experiments," *IEEE Trans. Electron Devices*, vol. 34, no. 7, pp. 1590–1602, Jul. 1987.

[40] S. Choi et al., "Interface analysis of ultrathin SiO2 layers between c-Si substrates and phosphorus-doped poly-Si by theoretical surface potential analysis using the injection-dependent lifetime," *Prog. Photovolt., Res. Appl.*, vol. 29, no. 1, pp. 32–46, 2021.

[41] D. B. M. Klaassen, "A unified mobility model for device simulation—I. Model equations and concentration dependence," *Solid-State Electron.*, vol. 35, no. 7, pp. 953–959, 1992.

[42] D. B. M. Klaassen, "A unified mobility model for device simulation—II. Temperature dependence of carrier mobility and lifetime," *Solid-State Electron.*, vol. 35, no. 7, pp. 961–967, 1992.

[43] P. P. Altermatt, "Models for numerical device simulations of crystalline silicon solar cells—A review," *J. Comput. Electron.*, vol. 10, no. 3, pp. 314–330, 2011.

[44] Renewable Resource Data Center, National Renewable Energy Laboratory, 2004. [Online]. Available: http://rredc.nrel.gov/solar/spectra/am1.5/

[45] J. Schmidt, F. M. Schuurmans, W. C. Sinke, S. W. Glunz, and A. G. Aberle, "Observation of multiple defect states at silicon–silicon nitride interfaces fabricated by low-frequency plasma-enhanced chemical vapor deposition," *Appl. Phys. Lett.*, vol. 71, no. 2, pp. 252–254, 1997.

[46] W. T. R. W. Shockley and W. T. Read, Jr., "Statistics of the recombinations of holes and electrons," *Phys. Rev.*, vol. 87, no. 5, 1952, Art. no. 835.

[47] D. Zielke et al., "Contact passivation in silicon solar cells using atomic-layer-deposited aluminum oxide layers," *Physica Status Solidi (RRL)–Rapid Res. Lett.*, vol. 5, no. 8, pp. 298–300, 2011.

[48] F. Kløw, E. S. Marstein, and S. E. Foss, "Tunneling contact passivation simulations using Silvaco Atlas," *Energy Procedia*, vol. 77, pp. 99–105, 2015.

[49] M. J. Kerr and A. Cuevas, "General parameterization of Auger recombination in crystalline silicon," *J. Appl. Phys.*, vol. 91, no. 4, pp. 2473–2480, 2002.

[50] C. Zechner, P. Fath, G. Willeke, and E. Bucher, "Two-and three-dimensional optical carrier generation determination in crystalline silicon solar cells," *Sol. Energy Mater. Sol. Cells*, vol. 51, no. 3/4, pp. 255–267, 1998.

[51] T. Panda et al., "Impact of multi-busbar front grid patterns on the performance of industrial type c-Si solar cell," *Sol. Energy*, vol. 236, pp. 790–801, Apr. 2022.